# Spatial Evolution of Mixing Layers: Effects of Shear and Convection

MOHAMMED A. AZIM
Department of Mechanical Engineering
Bangladesh University of Engineering and Technology, Dhaka-1000, BANGLADESH
email: azim@me.buet.ac.bd

*Abstract:* This paper has reported the effects of shear velocity, convection velocity and shear rate on the spatial evolution of turbulent axisymmetric mixing layers. The types of mixing layers investigated are with the variation of convection velocity under the constant shear velocity, with the variation of shear velocity under the constant convection velocity and with the variation of shear or convection velocity under the constant shear rate. The closed form equations governing the mixing layer flows are obtained by the standard $k-\varepsilon$ model and solved by using Fully Implicit Scheme and TDMA (Tridiagonal Matrix Algorithm). Obtained results show that the mixing layer thickness and momentum thickness evolve streamwise, and the shape and level of mean velocity, turbulent shear stress, mean vorticity and turbulence kinetic energy evolve streamwise but not radially with the changes in operating conditions at constant rate of shear. While changes in operating conditions affect the evolution of mixing layers in both directions under the constant shear or convection velocity.

*Key-Words:* Axisymmetric mixing layer, Turbulent flow, Spatial evolution, Shear velocity, Convection velocity, Shear rate, Computational fluid dynamics.

## 1 Introduction

Fundamental and practical significance of mixing layers have resulted in huge theoretical, experimental and numerical research. Common technological occurrences of mixing layers are, for example, in combustion chambers, premixers of gas turbine combustors, chemical lasers, flow reactors and propulsion systems. A mixing layer forms at the interface of two uniform streams of different velocity. As the two streams come in contact, the Kelvin-Helmholtz instability creates spanwise large-scale coherent vortices. These large-scale organized vortical structures in the mixing layers play an important role in the momentum and energy transport, particle dispersion and species diffusion. Such mixing layers develop through two successive distinct regions that is an initial region followed by a self-similar region. Based on geometrical configuration, turbulent mixing layers are of two types: plane mixing layer and axisymmetric mixing layer. Comparison shows close similarity between the axisymmetric mixing layer characteristics and those of the plane mixing layer [1]. Figure 1 illustrates an axisymmetric mixing layer.

Mixing layers are inherently very sensitive to small changes in their initial and operating conditions. There have been plenty of research on the factors affecting the evolution of mixing layer, some of them are: initial and boundary conditions [2,3], periodic oscillation force [4] and velocity ratio [5,6]. Despite that there is scarcity of publication regarding the effects of shear (velocity), convection (velocity) and shear rate on the evolution of mixing layer. Ho and Huang [7] studied two types of mixing layers, one is by the variation of low speed stream velocity while the high speed stream velocity is constant, and other is by the variation of velocity

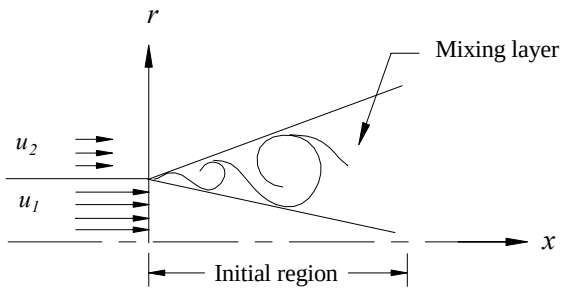


Fig. 1 Schematic of an axisymmetric mixing layer.

ratio while the shear velocity is constant. There occurred no significant change in the most amplified passage frequency in the former case but occurred significant change in the latter one. This passage frequency was found to dominate the flow dynamics. Further, they described the low speed side as not to be playing active role in the flow dynamics. On the other hand, some researchers, e.g. Slessor et al [3], argued that initial conditions of both high and low speed sides contribute into the initial region of the mixing layer. According to

many researchers, e.g. Roshko [8] and Oguchi and Inoue [9], mixing layer characteristics are dominated by the presence of spanwise vortical structures which are generated by the shear between the two fluid streams of different velocity.

Although most of the research on mixing layers are primarily experimental, there are considerable amount of research using numerical simulations. Methods used in the simulations of mixing layers are: closure model based on time-averaged properties [10], vortex method [11], large eddy simulation [12] and direct numerical simulation [13]. The findings of the numerical simulations, in general, are in good agreement with the existing experimental data.

Yang et al [12] from their investigation on the plane mixing layer presented the results of the effects of convection velocity and shear rate on the evolution of vortex structures, self-similarity and momentum thickness. They showed that momentum thickness is mainly dominated by the large vortex structure and their paring, and rate of shear has significant effects on the evolution of the flow while convection velocity has a little effect, and also the rate of shear and convection velocity have no significant effect on the normalized turbulence statistics.

In this paper, spatial evolution of axisymmetric turbulent mixing layers have been investigated numerically and the effects of shear velocity, convection velocity and shear rate on their properties have been reported. Present research is motivated by the lack in literature on the effects of those parameters on the evolution of mixing layers. In order to investigate, Reynolds Averaged Navier-Stokes (RANS) equations with the standard $k-\varepsilon$ turbulence model are solved where $k$ is turbulence kinetic energy and $\varepsilon$ is dissipation rate of $k$.

## 2 Governing Equations

Axisymmetric turbulent mixing layer flow is governed by the equations of continuity and RANS. Continuity equation and RANS equations in generic form for two-dimensional (2D) flow $\left(\bar{v},0,\bar{u}\right)$ in ($r$, $\theta$, $x$) co-ordinates by the assumptions of thin shear layer, uniform pressure and constant fluid property are

$$\frac{1}{r}\frac{\partial}{\partial r}\left(r\bar{v}\right)+\frac{\partial\bar{u}}{\partial x}=0 \tag{1}$$

$$\bar{v}\frac{\partial\phi}{\partial r}+\bar{u}\frac{\partial\phi}{\partial x}=\frac{1}{r}\frac{\partial}{\partial r}\left(vrN_{\phi}\frac{\partial\phi}{\partial r}\right)+S_{\phi} \tag{2}$$

where $\phi$ is the general flow variable that may represent $\bar{u}$, $k$ and $\varepsilon$. The transport coefficient $N_{\phi}$ and the source term $S_{\phi}$ in their full form are given in Table 1. In this 2D flow azimuthal mean vorticity component is

$$\Omega_{\theta}=1/2\left(\frac{\partial\bar{v}}{\partial x}-\frac{\partial\bar{u}}{\partial r}\right) \tag{3}$$

and other vorticity components are zero.

Table 1: The expressions of $N_{\phi}$ and $S_{\phi}$

| $\phi$ | $N_{\phi}$ | $S_{\phi}$ |
|---|---|---|
| $u$ | $\left(v+v_t\right)/v$ | $0$ |
| $k$ | $\left(v+v_t/\sigma_k\right)/v$ | $v_t\left(\partial\bar{u}/\partial r\right)^2-\varepsilon$ |
| $\varepsilon$ | $\left(v+v_t/\sigma_{\varepsilon}\right)/v$ | $C_{\varepsilon 1}v_t\left(\varepsilon/k\right)\left(\partial\bar{u}/\partial r\right)^2-C_{\varepsilon 2}\varepsilon^2/k$ |

### 2.1 Initial and boundary conditions

The conditions at the initiation are $\bar{u}\left(r\le r_o,0\right)=u_1$, $\bar{u}\left(r>r_o,0\right)=u_2$, $\bar{v}\left(r,0\right)=0$, $\overline{u'v'}\left(r,0\right)=0$, $k\left(r\le r_o,0\right)=0.001u_s^2$, $\varepsilon\left(r\le r_o\right)=k^{3/2}\left(0.3r_o\right)^{-1}$ and $k\left(r>r_o\right)=\varepsilon\left(r>r_o\right)=0$ where $r_o$ is the jet radius, and $u_1$ and $u_2$ are the uniform jet exit velocity and external air stream velocity, and also referred to as high speed and low speed stream velocities, respectively, and $u_s=u_1-u_2$. All the flow variables attain the uniform stream conditions at the edge of the mixing layer.

### 2.2 Turbulence closure

In the standard $k-\varepsilon$ model [14] for achieving turbulence closure, eddy viscosity is expressed by the Kolmogorov-Prandtl relation as

$$v_t=C_{\mu}k^2/\varepsilon \tag{4}$$

and the closure coefficients in this model are $C_{\mu}=0.09$, $\sigma_k=1.0$, $\sigma_{\varepsilon}=1.3$, $C_{\varepsilon 1}=1.44$ and $C_{\varepsilon 2}=1.92$.

## 3 Numerical Procedure

The governing equations (1)-(2) are solved using second order accurate Fully Implicit Scheme [15]

and TDMA [16]. Schematic of the computational domain of the present work is shown in Fig. 1. Grid spacing are uniform in *x*- direction with $\Delta x = 1.193\Delta r_1$ and variable in *r*- direction such that $\Delta r_{j+1} = K\Delta r_j$ and

$$\Delta r_1 = r_o(K-1)/\left(K^{nj-1}-1\right) \quad (5)$$

where *nj* is the number of grid points over $r_o$ and $K=1.02$. The under-relaxation factors used for $\bar{u}$-velocity, $\bar{v}$-velocity, turbulence kinetic energy and energy dissipation rate are *0.6, 0.6, 0.8* and *0.8*, respectively.

### 3.1 Grid convergence test

Grid convergence test is carried out with the three different grid sizes termed as coarse, medium and fine for *nj* equal to *11*, *16* and *21*, respectively. Figure 2 shows the profiles of mean streamwise

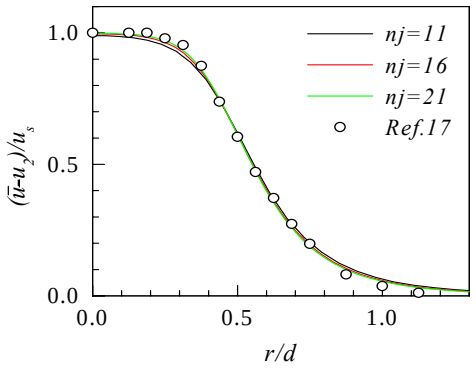


Fig. 2 Mean velocity profiles at $x/d=3$.

velocity of an axisymmetric jet at the location of $x/d=3$ for the three different grid resolutions where *d* is the jet diameter at exit. The experimental mean velocity data [17] appeared in this figure is discussed in the next section. The results corresponding to the coarse mesh have deviated to some extent compared to those obtained using medium and fine meshes. However, the results with medium and fine grid resolutions are very close to each other and the results presented in this paper are obtained by using the fine grid.

## 4 Results and Discussion

Equations (1)-(2) are solved numerically for the given initial and boundary conditions in Section 2.1 for the axisymmetric mixing layers. Fully Implicit Scheme and TDMA are used here successfully as computational tools. To examine the effectiveness of the numerical scheme, results from present simulation for circular air jet in quiescent ambient are compared with the experimental data [17]. The simulation is made for circular air jet in quiescent ambient with *40 mm* exit diameter and *12 m/s* top hat efflux velocity. The experimental jet was made for circular jet with *300 mm* diameter and *11 m/s* efflux velocity for unspecified initial turbulence level. In Fig. 2, mean velocity data at $x/d=3$ are found in close agreement with that of present simulation. The types of mixing layers studied here are given in Table 2 with their operating conditions (values of $u_1$ and $u_2$) where $u_s=u_1 - u_2$ is the shear velocity, $u_c=(u_1+u_2)/2$ is the convection velocity and $\lambda=u_s/u_c$ is the rate of shear. Growths of mixing layer thickness and momentum thickness, cross-stream variations of mean velocity, Reynolds shear stress, mean vorticity and turbulent kinetic energy, and streamwise evolution of shear stress, mean vorticity and kinetic energy maxima are presented in this section for the three types of mixing layers.

Table 2: Types of axisymmetric mixing layers

| *Type* | $u_1$(m/s) | $u_2$(m/s) | $u_s$(m/s) | $u_c$(m/s) | $\lambda$ |
|---|---|---|---|---|---|
| | *14.28* | *4.28* | | *9.28* | *1.08* |
| *1* | *21.66* | *11.66* | *10* | *16.66* | *0.6* |
| | *30* | *20* | | *25* | *0.4* |
| | *24* | *16* | *8* | | *0.4* |
| *2* | *26* | *14* | *12* | *20* | *0.6* |
| | *30.78* | *9.22* | *21.56* | | *1.08* |
| | *15* | *4.5* | *10.5* | *9.75* | |
| *3* | *20* | *6.0* | *14* | *13.0* | *1.08* |
| | *30* | *9.0* | *21* | *19.5* | |

### 4.1 Mixing layer thickness

It represents the flow width where fluid dynamical mixing activity occurs and defined as

$$\delta = y_{0.1} - y_{0.95} \quad (6)$$

where $y_{0.1}$ and $y_{0.95}$ are the isovels at $u_*$ equals *0.1* and *0.95*, and $u_* = \left(\bar{u}-u_2\right)/u_s$. Mixing layer thicknesses for the three types of mixing layers are shown in Fig. 3(a)-(c) where the thicknesses have grown linearly for some distance downstream. Entrainment of fluids from uniform streams, and pairing and amalgamation of the vortices are responsible for the growth of the mixing layers. In Fig. 3(a), the growth has reduced with increasing convection velocity under the constant shear as the

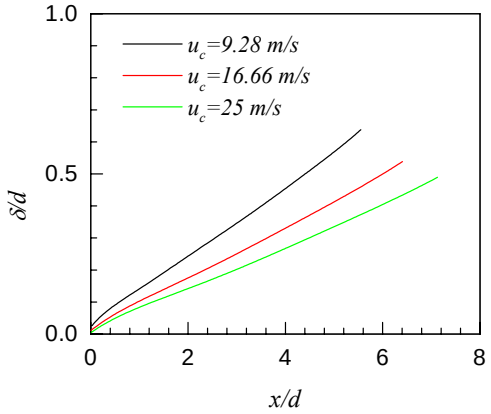


Fig. 3(a) Mixing layer thickness for $u_s$=10 m/s.

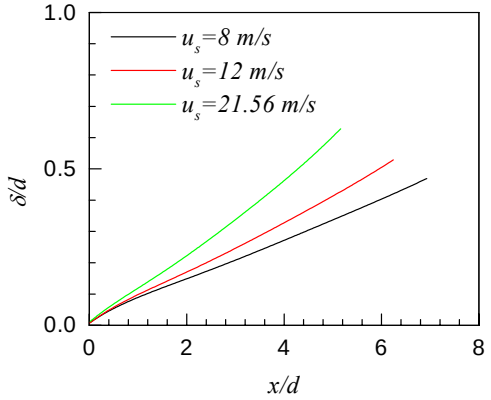


Fig. 3(b) Mixing layer thickness for $u_c$=20 m/s.

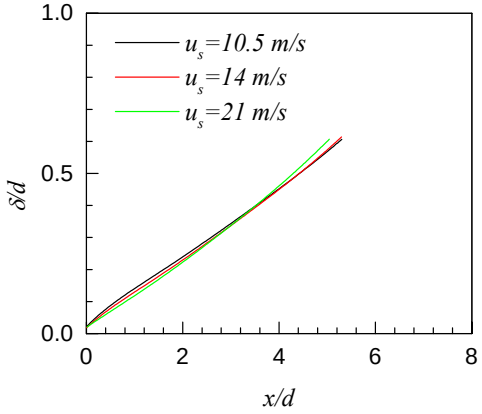


Fig. 3(c) Mixing layer thickness for $\lambda$=1.08.

vortices get less time for entrainment, pairing and amalgamation at any streamwise location. In Fig. 3(b), the growth of mixing layer has increased with increasing shear velocity under constant convection as vortical structures get larger directly with the increased shear velocity. Figure 3(c) shows that mixing layer thicknesses are not affected at constant shear rate because the increase in growth due to increasing shear velocity is offset by the decrease in growth due to increasing convection velocity.

## 4.2 Momentum thickness

It is the measure of momentum loss in the flow and expressed as

$$\theta = \int_0^\infty u*(1-u*)dr\,. \qquad (7)$$

Momentum thickness and mixing layer thickness as well are important parameters for characterizing the mixing layer flow. The distributions of momentum thicknesses for the three types of mixing layers are shown in Fig. 4(a)-(c) where the thicknesses have grown linearly for some distance downstream. In Fig. 4(a), the growth of momentum thickness has decreased with increasing convection velocity under

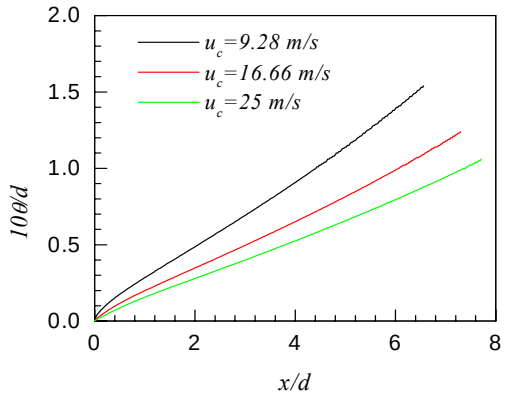


Fig. 4(a) Momentum thickness for $u_s$=10 m/s.

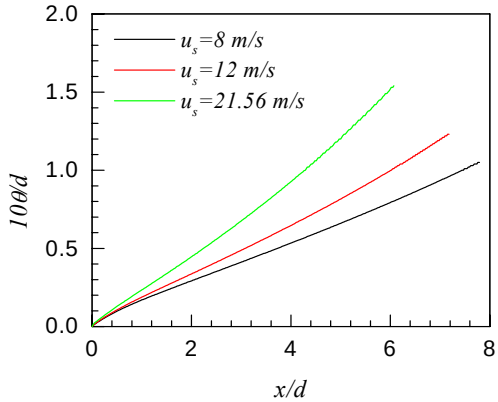


Fig. 4(b) Momentum thickness for $u_c$=20 m/s.

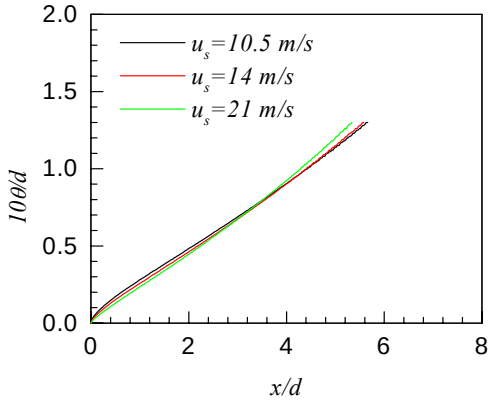


Fig. 4(c) Momentum thickness for $\lambda=1.08$.

the constant shear velocity as the loss of momentum reduces with increasing convection velocity due to the reduction in entrainment. In Fig. 4(b), growth of the momentum thickness has increased with increasing shear velocity under constant convection as increased shear velocity causes increase in momentum loss due to increasing lateral diffusion. Figure 4(c) shows that increase in momentum thickness due to the increasing shear velocity is offset by the decrease in growth due to increasing convection at constant rate of shear. Yang et al [12] have shown with the same rate of shear that the growths of momentum thicknesses are not affected by the change in convection velocity. But they have not considered the effect of convection under the constant shear velocity.

### 4.3 Streamwise mean velocity

Normalized mean velocity $\left(\overline{u}-u_2\right)/u_s$ is plotted in Fig. 5(a)-(c) against the radial distance *r/d* at the axial location *x/d=3* for the three types of mixing layers. Figure 5(a) shows that development distance of the flow increases with increasing convection under the constant shear velocity because the flow get less time to develop. Figure 5(b) shows that the development distance decreases with increasing shear under the constant convection velocity because the growth of large structures due to increasing shear is fed by the mean motion decay. On the other hand, Fig. 5(c) shows that the development distance remains unaffected at constant rate of shear under increasing convection and shear velocity because reduction in development distance due to the increased

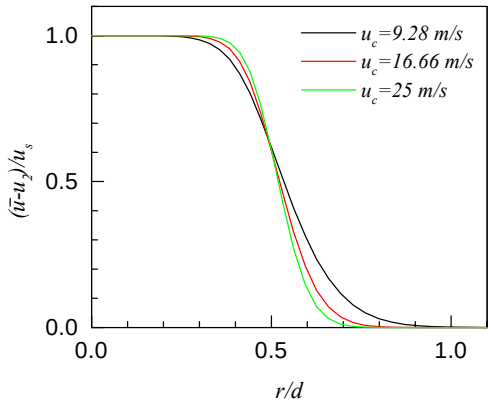


Fig. 5(a) Mean streamwise velocity profiles at *x/d=3* for $u_s$=10 m/s.

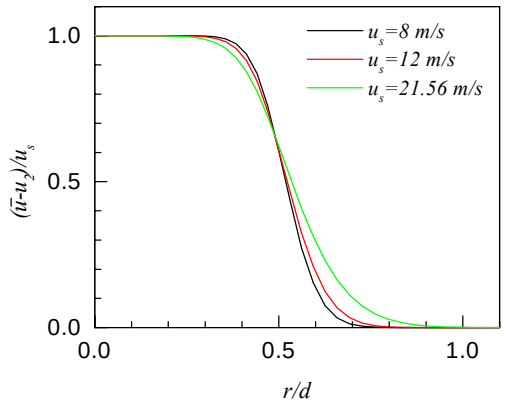


Fig. 5(b) Mean streamwise velocity profiles at *x/d=3* for $u_c$=20 m/s.

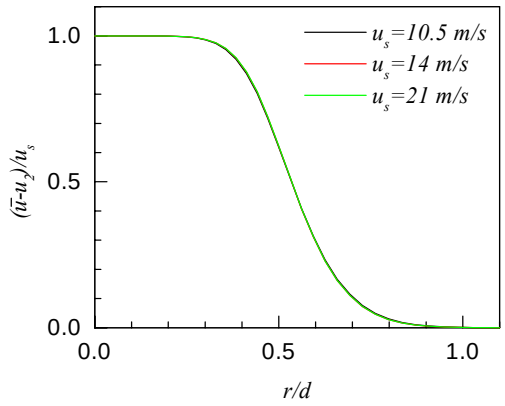


Fig. 5(c) Mean streamwise velocity profiles at *x/d=3* for $\lambda=1.08$.

shear velocity is offset by the increase in development distance due to the increased convection velocity.

### 4.4 Reynolds shear stress

The profiles of Reynolds shear stress $\overline{u'v'}/u_s^2$ are plotted as a function of radial distance *r/d* at the axial location *x/d = 3* in Fig. 6(a)-(c) for the three types of mixing layers. The level of $\overline{u'v'}$ profile is mostly dependent on the intensity of shear interaction. In Fig. 6(a), increasing convection under

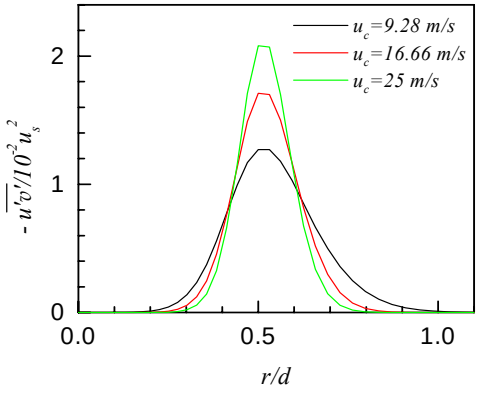


Fig. 6(a) Reynolds shear stress profiles at *x/d=3* for $u_s$*=10 m/s*.

the constant shear velocity causes increasing interaction between mean motion and turbulence leading to increasing shear stress. In Fig. 6(b), increasing shear velocity under constant convection causes vortical structures to grow larger and to reduce in coherence that result in reduced level of

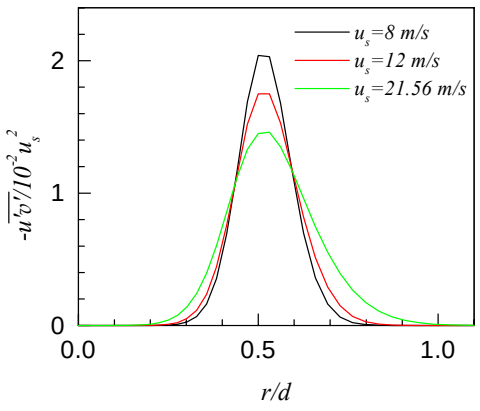


Fig. 6(b) Reynolds shear stress profiles at *x/d=3* for $u_c$*=20 m/s*.

shear stress. Figure 6(c) shows that shear stress remains unchanged at constant rate of shear because reduction in stress due to the increased shear velocity is offset by the increase in stress due to the increased convection velocity.

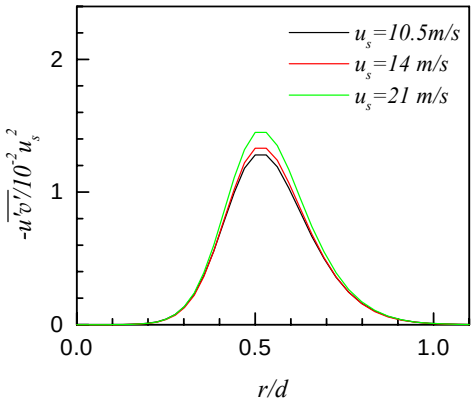


Fig. 6(c) Reynolds shear stress profiles at *x/d=3* for $\lambda$*=1.08*.

### 4.5 Mean vorticity

Normalized mean vorticity $\Omega_\theta d/u_s$ is shown in Fig. 7(a)-(c) against the radial variation at *x/d = 3* for the three types of mixing layers where $\Omega_\theta$ is calculated from Eq. (3). In Fig. 7(a) for the constant

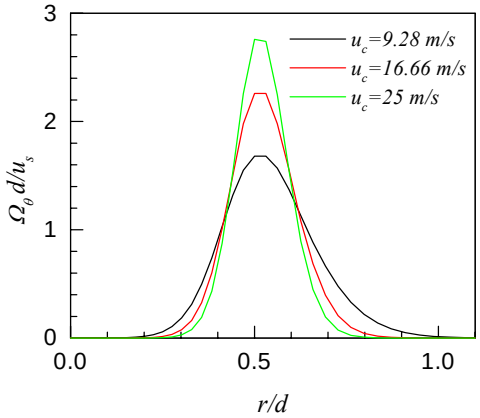


Fig. 7(a) Mean vorticity profiles at *x/d=3* for $u_s$*=10 m/s*.

shear velocity, increasing convection velocity causes increased level of vorticity by the reduction of both non-turbulent entrainment and vortices amalgamation. In Fig. 7(b) for the constant

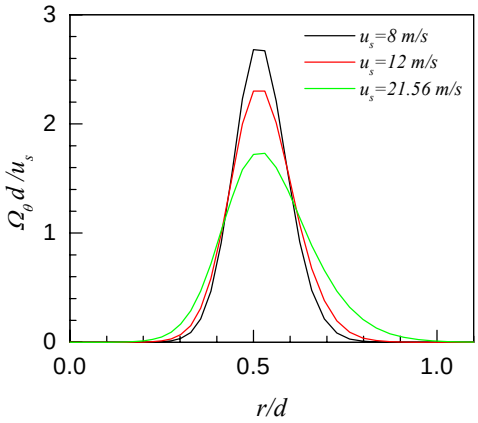


Fig. 7(b) Mean vorticity profiles at *x/d=3* for $u_c$*=20 m/s*.

convection velocity, increasing shear velocity causes vortices to grow larger leading to reduced level of vorticity. Figure 7(c) shows that the level of mean vorticity remains unaffected at constant shear rate for different shear or convection velocity, because reduction in vorticity due to the increased shear velocity is offset by the increase in vorticity due to the increased convection velocity.

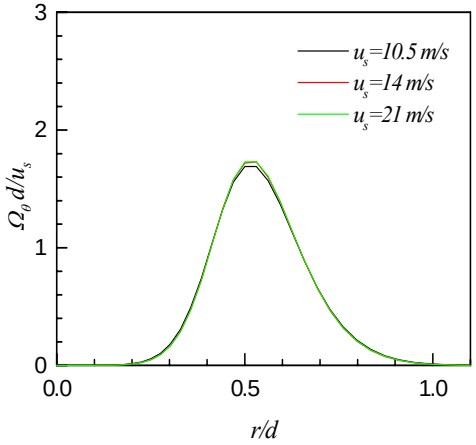


Fig. 7(c) Mean vorticity profiles at *x/d=3* for *λ=1.08.*

## 4.6 Turbulent kinetic energy

Normalized turbulent kinetic energy $k/u_s^2$ is shown against the radial variation in Fig. 8(a)-(c). The effects of shear velocity, convection velocity and shear rate on the turbulence kinetic energy profiles are found similar to the turbulent shear stress

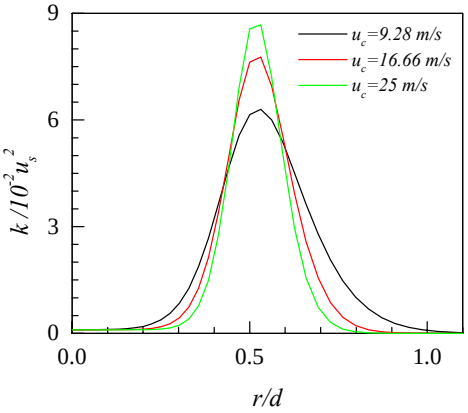


Fig. 8(a) Kinetic energy profiles at *x/d=3* for $u_s$*=10 m/s*.

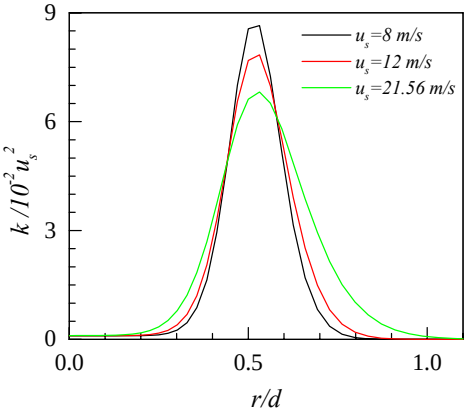


Fig. 8(b) Kinetic energy profiles at *x/d=3* for $u_c$*=20 m/s*.

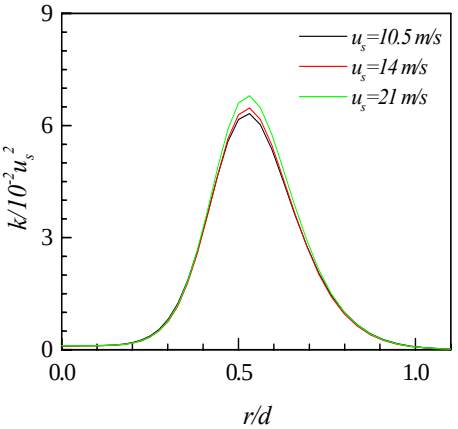


Fig. 8(c) Kinetic energy profiles at *x/d=3* for *λ=1.08.*

because this stress contributes directly to the production of $k/u_s^2$.

### 4.7 Mean and turbulence quantities maxima

Streamwise evolution of the normalized shear stress, mean vorticity and kinetic energy maxima for the three types of mixing layers are shown in Figs. 9-11.

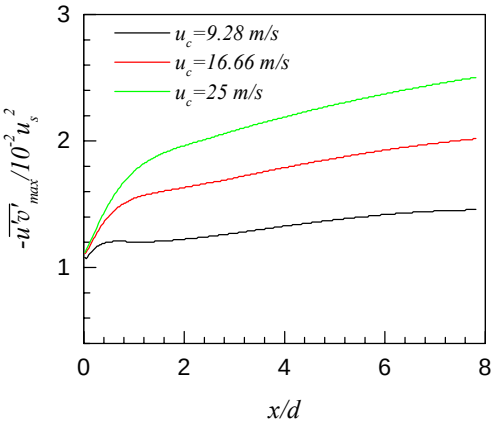


Fig. 9(a) Axial variation of shear stress maxima for $u_s$=10 m/s.

In the initial region of the mixing layers ($x/d \le 8$), Fig. 9(a)-(c) shows that $\overline{u'v'}_{max}/u_s^2$ increases in the downstream due to increasing shear interaction between the decaying mean motion and turbulence, Fig. 10(a)-(c) shows that $\Omega_{\theta max}d/u_s$ decreases due to entrainment of non-turbulent fluid in the downstream, and Fig. 11(a)-(c) shows that turbulent kinetic energy increases in the downstream similarly

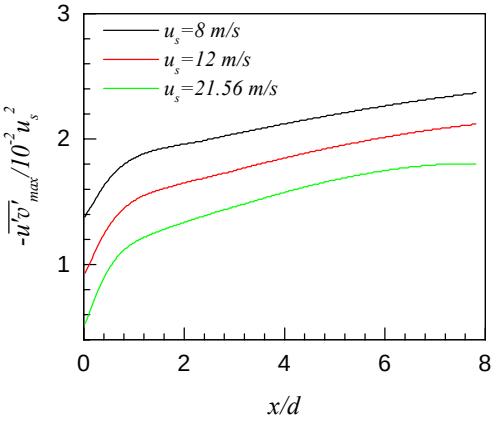


Fig. 9(b) Axial variation of shear stress maxima for $u_c$=20 m/s.

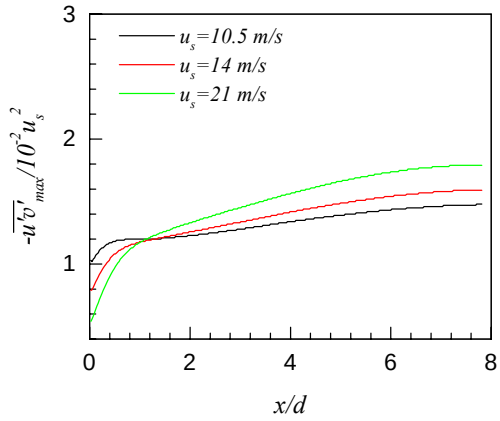


Fig. 9(c) Axial variation of shear stress maxima for $\lambda$=1.08.

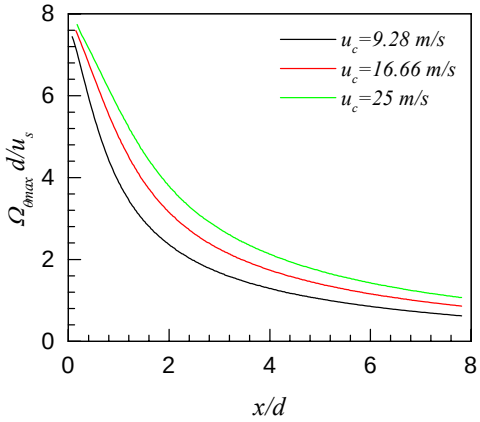


Fig. 10(a) Axial variation of mean vorticity maxima for $u_s$=10 m/s.

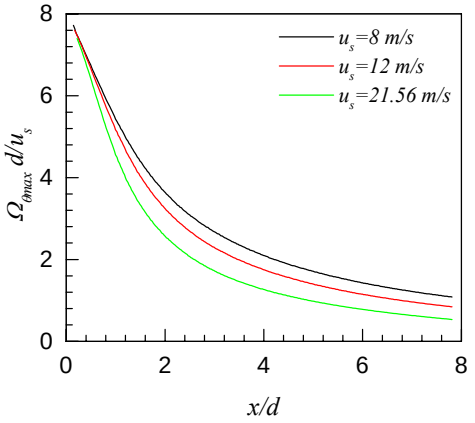


Fig. 10(b) Axial variation of mean vorticity maxima for $u_c$=20 m/s.

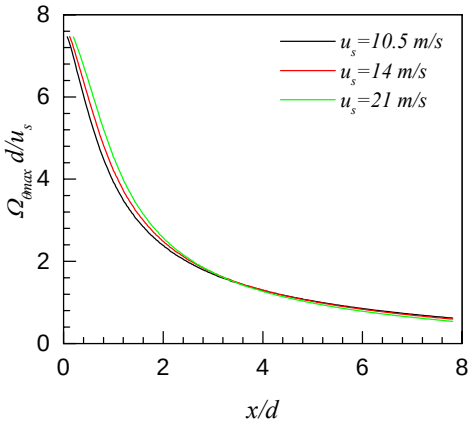


Fig. 10(c) Axial variation of mean vorticity maxima for $\lambda=1.08$.

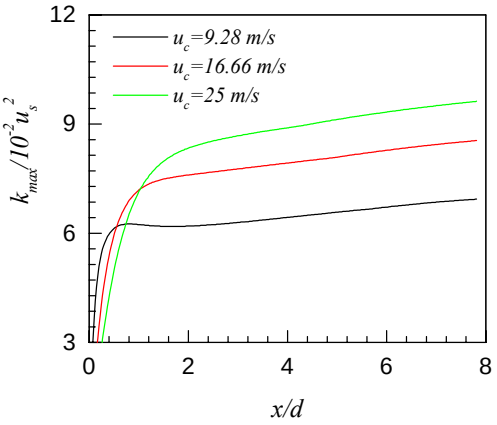


Fig. 11(a) Axial variation of kinetic energy maxima for $u_s=10$ m/s.

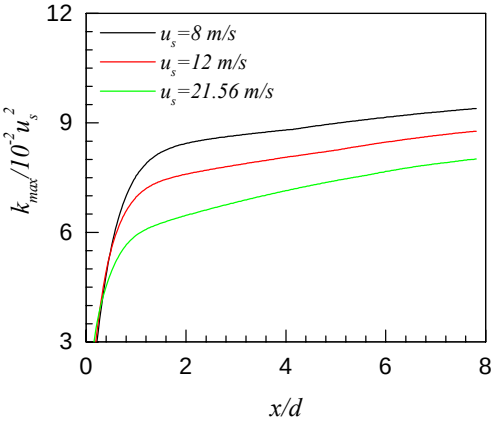


Fig. 11(b) Axial variation of kinetic energy maxima for $u_c=20$ m/s.

as turbulent shear stress because it contributes directly to the production of $k/u_s^2$. The effects of shear velocity, convection velocity and shear rate on the levels of turbulent shear stress, mean vorticity and turbulent kinetic energy have already been discussed.

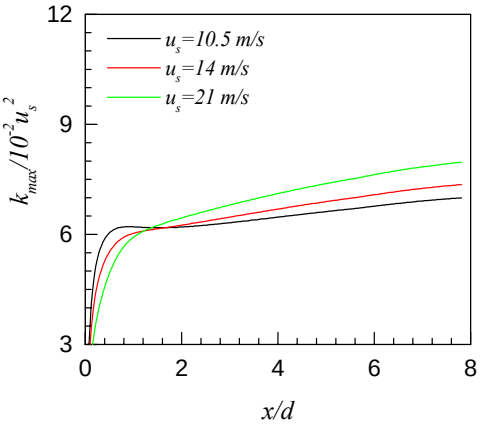


Fig. 11(c) Axial variation of kinetic energy maxima for $\lambda=1.08$.

## 5 Conclusions

Three types of axisymmetric turbulent mixing layers, as shown in Table 2, have been investigated to evaluate the effects of shear velocity, convection velocity and shear rate on their spatial evolution. The equations governing the mixing layer flow for the given initial and operating conditions are solved using Fully Implicit Scheme and TDMA. Results of the present simulations show that the growths of mixing layer thickness, momentum thickness and development distance of the flow, and the radial evolution in shape and level of the mean velocity, shear stress, mean vorticity and kinetic energy are not affected by the changes in operating conditions under the constant shear rate. While increasing convection velocity under the constant shear velocity causes reduction in the growths of mixing layer thickness and momentum thickness, and increase in the development distance of the flow, and increase in shape and level of the shear stress, mean vorticity and kinetic energy, and the reverse is true for the mixing layer with increasing shear velocity under constant convection. So regarding the normalized turbulence statistics, there is significant discrepancy between the claims of Yang et al [12] and the findings of the present simulations.

*References:*


[1] A. K. M. F. Hussain, Z. D. Husain, Turbulence Structure in the Axisymmetric Free Mixing Layer, *AIAA Journal,* Vol.18, 1980, pp. 1462-1469.

[2] J. H. Bell, R. D. Mehta, Development of a Two-Stream Mixing Layer with Tripped and Untripped Boundary Layers, *AIAA Journal,* Vol.28, 1990, pp. 2034-2042.

[3] M. D. Slessor, C. L. Bond, P. E. Dimotakis, Turbulent Shear Layer Mixing at High Reynolds Numbers: Effects of Inflow Conditions, *J. Fluid Mech*., Vol.376, 1998, pp. 115-138.

[4] D. Oster, I. J. Wygnanski, The Forced Mixing Layer between Parallel Streams, *J. Fluid Mech.,* Vol.123, 1982, pp. 91-130.

[5] R. D. Mehta, Effects of Velocity Ratio on Plane Mixing Layer Development: Influence of the Splitter Plate Wake, *Exp. Fluids,* Vol.10, 1991, pp. 194-204.

[6] F. Guo, B. Chen, L. Guo, X. Zhang, Effects of Velocity Ratio on Turbulent Mixing Layer at High Reynolds Number, *J. Phys.: Conference Ser.* 147, 2009, pp. 1-6.

[7] C. M. Ho, L. S. Huang, Sub-Harmonics and Vortex Merging in Mixing Layers, *J. Fluid Mech*., Vol. 119, 1982, pp. 443-473.

[8] A. Roshko, The Plane Mixing Layer Flow Visualization Results and Three-Dimensional Effects, *Lecture Note in Physics,* Vol.136, 1980, pp. 208-217.

[9] H. Oguchi, O. Inoue, Mixing Layer Produced by a Screen and Its Dependence on Initial Conditions, *J. Fluid Mech*., Vol.142, 1984, pp. 217-231.

[10] R. D. Mehta, O. Inoue, L. S. King, J. H. Bell, Comparison of Experimental and Computational Techniques for Plane Mixing Layers, *Phys. Fluids,* Vol.30, 1987, pp. 2054-2062.

[11] P. S. Bernard, Grid-Free Simulation of the Spatially Growing Turbulent Mixing Layer, *AIAA Journal,* Vol.46, No.7, 2008, pp. 1725-1737.

[12] W. B. Yang, H. Q. Zhang, C. K. Chan, K. S. Lau, W. Y., Lin, Investigation of Plane Mixing Layer Using Large Eddy Simulation, *Computational Mech*., Vol.34, 2004, pp. 423-429.

[13] M. J. Maghrebi, A. Zarghami, DNS of Forced Mixing Layer, *Int. J. Numer. Analysis and Modeling,* Vol.7, No.1, 2010, pp. 173-193.

[14] B. E. Launder, D. B. Spalding, The Numerical Computation of Turbulent Flows, *Comput. Methods in Appl. Mech. Eng.,* Vol.3, 1974, pp. 269-289.

[15] D. A. Anderson, J. C. Tannehill, R. H. Pletcher, *Computational Fluid Mechanics and Heat Transfer*, McGraw-Hill, New York, 1984.

[16] L. H. Thomas, Elliptic Problems in Linear Difference Equations Over a Network, *Watson Sci Comput Lab Report,* Columbia University, New York, 1949.

[17] S. Sami, T. Carmody, H. Rouse, Jet Diffusion in the Region of Flow Establishment, *J. Fluid Mech*., Vol.27, 1967, pp. 231-252.